

Imaging nuclei by smashing them at high energies: how are their shapes revealed after destruction?

Jiangyong Jia^{1,2,*}

¹*Department of Chemistry, Stony Brook University, Stony Brook, NY 11794, USA*

²*Physics Department, Brookhaven National Laboratory, Upton, NY 11976, USA*

High-energy nuclear collisions were recently employed as an “imaging-by-smashing” tool to reveal the global shapes of colliding nuclei. Here, I explain how nuclear shapes become encoded during quark-gluon plasma formation and evolution, and how they can be decoded from final-state particle distributions. I highlight the method’s potential to advance our understanding of both nuclear structure and quark-gluon plasma physics.

In many areas of science, imaging relies on external probes, often photons, to interact with samples and extract structural details. The scattered probe encodes the sample’s structure, much like in X-ray crystallography, where a molecule’s three-dimensional arrangement is inferred from scattering patterns in momentum space. In such methods, imaging takes place as the probe traverses the sample, and because any structural disintegration happens only after scattering, the captured information remains intact.

A markedly different approach has emerged in nuclear physics: Instead of using external probes, atomic nuclei of interest are collided at ultra-high energies to form a hot, dense state of matter known as the quark-gluon plasma (QGP). The geometric structure of the colliding nuclei determines the QGP’s initial condition and influences its subsequent evolution, ultimately imprinting specific patterns on the momenta of the final-state particles. By “rewinding” this evolution, one could reconstruct an effective image of the original nuclei.

Using this strategy, the STAR Collaboration extracted the shape of ^{238}U by analyzing $^{238}\text{U}+^{238}\text{U}$ collisions [1]. Although these collisions completely destroy the nuclei, their structural information is preserved with sufficient detail to allow such a reconstruction. This finding raises a fundamental question: How are nuclear shapes encoded in high-energy collisions, and how can they be deduced from the resulting final-state particles? The present discussion aims to explore this question and the broader implications of the technique.

Traditional methods for nuclear shapes Atomic nuclei are bound systems of protons and neutrons (nucleons), held together by the strong nuclear force. Although often depicted as spheres, they can adopt prolate, oblate, or even pear-like configurations – shapes governed by the underlying many-body wavefunction. This wavefunction governs the positions and momenta of nucleons. Because theoretical predictions of these shapes are challenging, experimental input is crucial.

Unlike molecules, nuclei cannot be oriented in a crystalline lattice for direct coherent imaging. Instead, low-energy techniques such as electron scattering, Coulomb excitation (Coulx), and laser spectroscopy have traditionally been used to infer nuclear shapes [2]. Electron scattering probes nuclei one at a time, providing

an orientation-averaged image in which nuclear deformation manifests as modifications to the charge distribution. Coulx, a widely used technique, excites nuclei into rotational and vibrational states using low-energy ions. By detecting the gamma rays emitted when the nucleus relaxes to its ground state and comparing the data to theoretical models, its shape can be deduced.

However, these methods rely on electromagnetic interactions and thus do not directly probe neutron distributions. Moreover, the relatively long timescales involved yield time-averaged, blurred representations of nuclear shapes, akin to long-exposure photographs. As a result, such techniques are limited in their ability to resolve rapid fluctuations and dynamic variations in nuclear shapes.

Imaging-by-smashing at high energy High-energy nuclear collisions offer a fundamentally different way to image nuclei (Fig. 1d). The key timescale is set by the crossing time of the two colliding nuclei $\tau = 2R_0/\Gamma < 0.1\text{fm}/c$, where R_0 is the nuclear radius and $\Gamma > 100$ is the Lorentz contraction factor. Initially, the nuclear shape influences the conditions under which the QGP forms. As the plasma expands hydrodynamically, information about the nuclear shape is transformed and ultimately encoded in the momentum distribution of thousands of final-state particles. By carefully analyzing these distributions and rewinding the expansion event by event, the shape of nuclei can be reconstructed. Naturally, the precision of this method hinges on how well the initial condition, equation of state, and transport properties of the QGP are understood. These aspects have been the focus of the heavy-ion community for decades and are now believed to be well-constrained [3].

This imaging-by-smashing principle appears in other areas of physics covering a wide range of length scales, as shown in Fig. 1a–c. For example, elliptical or triangular water droplets colliding with hydrophobic surfaces undergo pressure-driven expansions that invert their shape asymmetries [4]. Strongly-coupled cold atomic Fermi gases exhibit similar behavior, with anisotropies in their initial state transformed and inverted in the final state [5]. Chemistry provides another parallel through Coulomb explosion imaging (CEI): by removing electrons from a molecule (using a laser or thin foil), one induces nuclear repulsion that can be “unwound” to reveal the

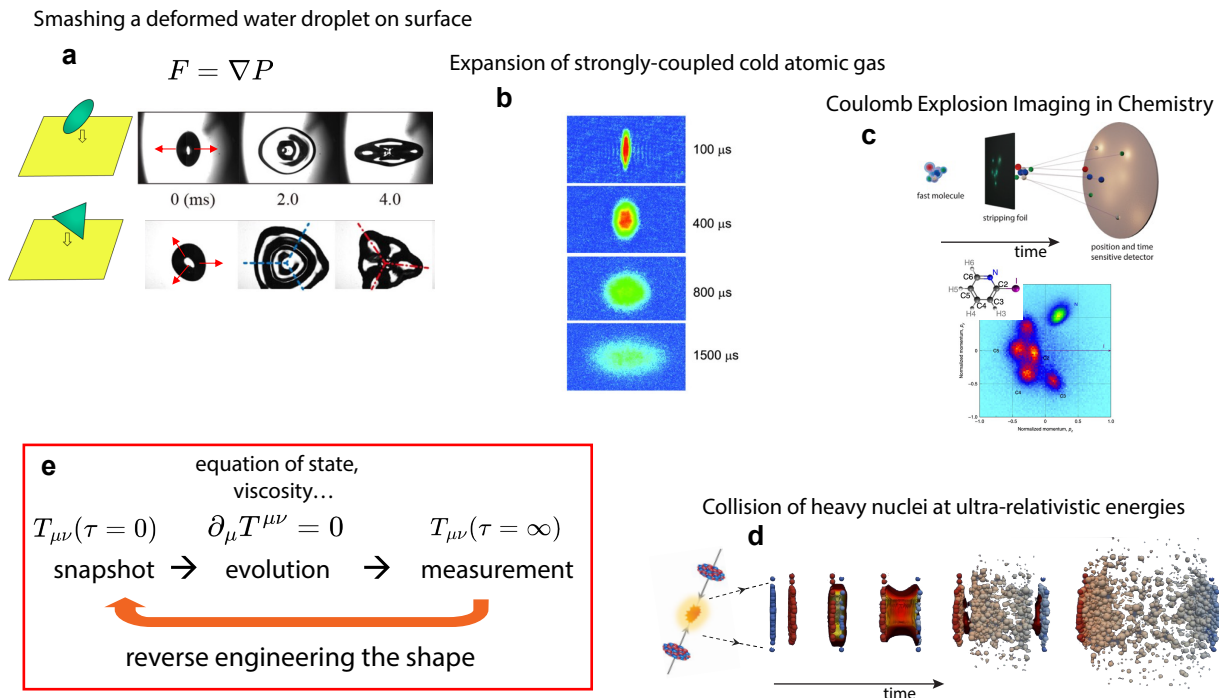


FIG. 1. **Connections between initial and final state in various “smashing” experiments:** (a) Deformed water droplet colliding with a hydrophobic surface, producing an expansion pattern that inverts the initial shape asymmetry [4]; (b) Expansion of a strongly-coupled Fermi gas released from an optical trap [5], whose geometry leaves imprints in the subsequent dynamics of the gas due to the ultra-fast switch-off of the confining potential; (c) Coulomb-explosion imaging of a small molecule stripped of electrons, in which nuclear positions are inferred by reversing the repulsive expansion [6, 7]; (d) Pressure-driven expansion of the quark-gluon plasma produced in high-energy nuclear collisions [3]. In each case, the final state can be reverse-engineered to extract the initial condition, provided the expansion dynamics, represented by the system’s energy-momentum tensor $T_{\mu\nu}$, are sufficiently well understood (e).

molecule’s spatial configuration [6, 7].

These examples share three essential features (Fig. 1e): an initial configuration to be imaged, collective expansion governed by well-defined evolution equations, and final state detection. Imaging then boils down to reverse-engineering the expansion to recover the original structure.

Although imaging by smashing nuclei at high energies may seem like an extreme approach, it does offer distinct advantages. First, the collision probes the ground state nuclear many-body wavefunction in position space, information not readily accessible by more conventional means. Second, the subsequent expansion is well described by classical hydrodynamics, an effective theory valid for systems with densely populated degrees of freedom (DOF), irrespective of their sizes. Moreover, high-energy collisions produce far more final-state particles per event than traditional experiments, allowing for more detailed reconstructions. In this sense, the process’s apparent destructiveness becomes an asset.

Energy dependence of the nuclear image The observed image of an atomic nucleus, and its effective many-body wavefunction, depends on the timescale at which it is probed, which is tied to the collision energy $\sqrt{s_{NN}}$ (Fig. 2). At low energies, where the “shutter speed” is ef-

fectively slow, collective rotational and vibrational DOF dominate the nucleus’s appearance. For instance, the rotational DOF of a deformed heavy nucleus, with excitation energies around 0.1 MeV, corresponds to timescales of $\tau \sim 10^3 - 10^4$ fm/c. As collision energy increases, faster modes such as nucleon clustering and short-range correlations come into play. At still higher energies, the resonance structure of nucleons emerges, eventually giving way to the subnucleonic quarks and gluons. The imaging process effectively captures all DOF slower than the nuclear crossing timescale, leaving any faster modes unresolved. As a result, varying $\sqrt{s_{NN}}$ provides a natural way to study the evolution of the nuclear wavefunction across energy scales.

While electron-nucleus scattering probes the one-body distribution of the scattering centers – protons at low energy and quarks and gluons at high energy – much less is known about the nuclear many-body distributions across broad energy scales. High-energy heavy-ion collisions help fill this gap. Measurements of anisotropic flow coefficients reveal quantum fluctuations associated with the finite number of scattering centers [8], inducing deformed nucleon distribution in the transverse (xy) plane, with eccentricities scaling roughly as $1/A$, where A is

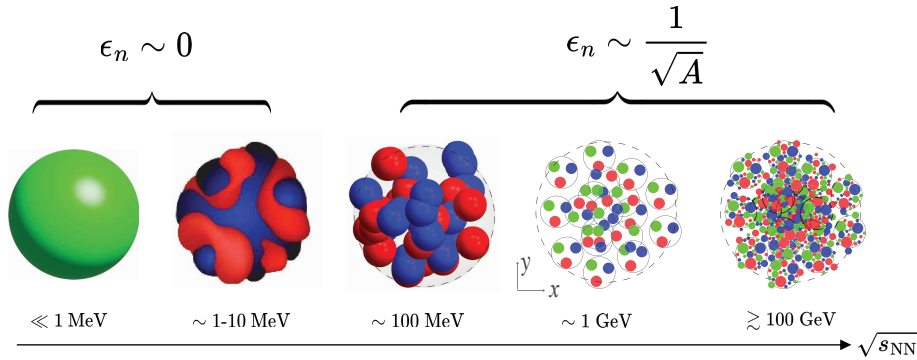


FIG. 2. **Energy dependence of nuclear structure.** Different degrees of freedom become relevant at different energies, affecting the apparent shape of the nucleus. Due to quantum fluctuations at nucleon and subnucleonic level, even a nominally spherical nucleus such as ^{208}Pb exhibits a deformed nucleon distribution in the transverse plane at high energies.

the mass number ¹. This fluctuation-driven deformation produces non-zero flow even in head-on collisions, where the nuclear overlap regions is isotropic on average (see Fig. 2).

From these considerations, one can infer that the image of an atomic nucleus at high energy possesses two distinct deformation components. The first reflects slow, global shape modes, such as rotational and vibrational, independent of collision energy. The second arises from quantum fluctuations at the nucleon and subnucleonic scales, which vary with $\sqrt{s_{\text{NN}}}$. A robust imaging method is essential for disentangling and studying each contribution separately. By comparing results from RHIC and the LHC, one can investigate the energy dependence of these two components in detail [9].

Reverse-engineering nuclear shape A nucleus with quadrupole deformation can be described by a surface function in terms of the polar angle θ and azimuthal angle ϕ ,

$$R(\theta, \phi) = R_0(1 + \beta_2(\cos \gamma Y_{2,0} + \sin \gamma Y_{2,2})), \quad (1)$$

where $Y_{l,m}(\theta, \phi)$ are spherical harmonics. The parameters β_2 and γ define the quadrupole deformation and triaxiality, respectively. The γ controls the ratios of principal radii. As γ varies from 0° to 60° , the nucleus transitions from prolate ($\gamma = 0^\circ$) to oblate ($\gamma = 60^\circ$), with intermediate values corresponding to triaxial shapes. Higher-order deformations, such as octupole β_3 or hexadecapole β_4 , can also be included but are typically much smaller than β_2 . When projected onto the xy -plane, these deformation components give rise to elliptic, triangular, or quadrangular initial geometries of the QGP [10].

Imaging nuclear shape at high energy involves a three-step process. First, the initial conditions of the collision

are reconstructed from final-state observables using hydrodynamic models that link measured particle distributions to the geometry of the QGP. Second, these initial conditions are mapped back to the intrinsic nuclear shape. Finally, by comparing two isobar-like collision systems – nuclei with similar mass but differing structural properties – global nuclear shape effects can be distinguished from fluctuations on nucleonic and subnucleonic scales.

Step 1: From the final state to the initial condition. Figure 3a illustrates how the QGP’s initial geometry in a single event is characterized by moments of its energy density distribution $T(x, y)$ in the transverse plane. Key parameters include the total energy $E = \int T(x, y) dx dy$, the elliptic and triangular eccentricities ε_2 and ε_3 , and inverse of mean-square area d_\perp :

$$d_\perp = 1/\sqrt{\langle x^2 \rangle \langle y^2 \rangle}, \quad \mathcal{E}_n \equiv \varepsilon_n e^{in\Phi_n} = -[(x + iy)^n] / [|(x + iy)|^n], \quad (2)$$

with “[.]” indicates averaging weighted by $T(x, y)$, and Φ_n represents the orientation of the n^{th} eccentricity.

The total energy E influences the number of produced charged particle. Meanwhile, the initial eccentricities ε_n drive anisotropic flow, described by $dN/d\phi \propto 1 + 2 \sum_n v_n \cos(n(\phi - \Psi_n))$, where v_n (with phase Ψ_n) define the elliptic (v_2) and triangular (v_3) flow coefficients (Fig. 3b). Additionally, d_\perp governs the radial expansion or “radial flow”, affecting the average transverse momentum $[p_T]$ of final-state particles. Hydrodynamic modeling suggests approximately linear relationships between these initial- and final-state observables: $v_n \propto \varepsilon_n$ and $\delta p_T/p_T \propto \delta d_\perp/d_\perp$ [11, 12]². The proportionality constants (response coefficients) are strongly impacted by QGP properties.

¹ The eccentricities are mostly determined by the positions of nucleons, as most quarks and gluons are confined within them and nuclear modifications are modest.

² Here, $\frac{\delta p_T}{p_T} = \frac{[p_T] - \langle [p_T] \rangle}{\langle [p_T] \rangle}$ and $\frac{\delta d_\perp}{d_\perp} = \frac{d_\perp - \langle d_\perp \rangle}{\langle d_\perp \rangle}$ denote event-by-event fluctuations, and “⟨.⟩” indicates average over events.

Extracting QGP properties, such as the equation of state and transport coefficients, has long been a major goal in heavy-ion physics. The state-of-the-art approach employs Bayesian analyses to simultaneously constrain these QGP parameters and the initial conditions [13]. However, uncertainties in the initial conditions still limit the precision of these extractions – a limitation that can be reduced by leveraging the collision of species with well-understood shapes [14].

Step2: from the initial condition to nuclear shape The QGP's initial condition is closely tied to the transverse distribution of nucleons in the colliding nuclei A and B, described by thickness functions $T_{A,B}(x, y)$, which fluctuate from event to event. In the presence of global deformation, these functions also depend on the nuclei's orientations prior to collision (see Fig. 4a1 and 4b1). For head-on collisions, random orientations of prolate deformed nuclei lead to significant but anti-correlated fluctuations between v_2 and $\langle p_T \rangle$ [15]. General considerations imply that such fluctuations follow simple parametric forms [16]. Specifically, the three moments used by the STAR Collaboration are

$$\begin{aligned}\langle v_2^2 \rangle &= a_1 + b_1 \beta_2^2, \\ \langle (\delta p_T)^2 \rangle &= a_2 + b_2 \beta_2^2, \\ \langle v_2^2 \delta p_T \rangle &= a_3 - b_3 \beta_2^3 \cos(3\gamma). \end{aligned} \quad (3)$$

Here a_n and b_n are positive coefficients that depend on the impact parameter. The a_n terms capture contributions from quantum fluctuations, explaining finite v_2 even at zero impact parameter, while the b_n terms reflect the response to global deformation.

Both a_n and b_n are influenced by how colliding nucleons deposit energy in the overlap region. In phenomenological applications, the energy density is typically parametrized in a flexible way from $T_{A,B}$, with those parameters inferred from experimental measurements. An oftenly used Ansatz is the generalized mean of the Trento model [17]:

$$T(x, y) = \left(\frac{T_A^p + T_B^p}{2} \right)^{q/p}, \quad (4)$$

where p and q set the energy deposition prescription, usually with $q = 1$.

In the simplest scenario of head-on collisions involving spherical nuclei, the initial density distribution closely follows the nucleon density distribution in the xy -plane: $T(x, y) \approx T_A \approx T_B$. Introducing a deformation perturbation along an Euler angle, $T_A = T_{A,0} + \delta_A(\Omega_A)$, one can show that the deformation effects are independent of parameter p , $T \approx T_0 + (\delta_A(\Omega_A) + \delta_B(\Omega_B))/2$. The spherical baseline $T_0(x, y)$ determines the a_n coefficients, while the deformation-induced perturbations $\delta(x, y)$ vary with the nuclear orientation and control the values of b_n . In this case, the initial geometry is determined mostly by

the nucleon distribution ³.

Additionally, both a_n and b_n vary with $\sqrt{s_{\text{NN}}}$. Gluon saturation effects at high energy tend to smooth out local fluctuations, reducing a_n . Conversely, the reduced central density could conceivably amplify the influence of nuclear deformation, increasing b_n .

Step3: Separating global deformation from quantum fluctuations The influence of nuclear deformation can be quite substantial. In head-on collisions of strongly-deformed uranium nuclei, the b_n terms in Eq. 2 can exceed 50% of the baseline fluctuation contribution for $\langle v_2^2 \rangle$ and $\langle (\delta p_T)^2 \rangle$, and up to three times for $\langle v_2^2 \delta p_T \rangle$ [1]. While one could in principle constrain deformation by comparing hydrodynamic model calculations with data in a single collision system, both a_n and b_n are strongly influenced by final-state effects, limiting the precision of this approach.

A more robust strategy involves comparing two collision systems of similar mass but different shapes. Ratios of bulk observables from these isobaric systems minimize sensitivity to QGP transport properties, thereby exposing differences rooted in the initial conditions and nuclear shapes. The STAR Collaboration used this approach to determine deformation parameters for ^{238}U by comparing collisions of ^{238}U (strongly deformed) and ^{197}Au (nearly spherical). For example, ratios of observables between a deformed nucleus and a spherical nucleus are:

$$\begin{aligned}R_{\langle v_2^2 \rangle} &= 1 + \frac{b_1}{a_1} \beta_2^2, \\ R_{\langle (\delta p_T)^2 \rangle} &= 1 + \frac{b_2}{a_2} \beta_2^2, \\ R_{\langle v_2^2 \delta p_T \rangle} &= 1 - \frac{b_3}{a_3} \beta_2^3 \cos(3\gamma). \end{aligned} \quad (5)$$

If the final-state responses for the a_n and b_n components are similar, the ratios b_n/a_n primarily reflect the nuclear shape and, to a lesser extent, the energy deposition process.

This three-step extraction procedure holds at collision energies of a few tens of GeV or higher, where the distinct stages of the collision – initial condition, QGP evolution, and freeze-out – occur on well-separated timescales. At lower energies of below a few GeV, these timescales overlap, necessitating the explicit treatment of nuclear structure in the initial conditions. Despite these complexities, isobaric comparisons remain a valuable tool for investigating the dynamics and properties of nuclear matter at lower energies. Deformed nuclei offer a unique way to globally rearrange nucleons, allowing collisions of such nuclei to probe the nuclear equation of state. The Fermi momenta of nucleons are also relevant to the measured

³ However, in non-head-on collisions or when $q \neq 1$, the linear dependence on nuclear deformation does not hold, and the relation between the initial energy distribution and nucleon distribution becomes non-trivial.

observables, leading to a more intricate interplay between nuclear structure and collision dynamics.

Imaging-by-smashing as a discovery tool The imaging-by-smashing technique offers exciting potential for advancing both heavy-ion and nuclear structure research [14]. Realizing its full potential, however, requires rigorous calibration and a thorough understanding of the QGP’s initial condition and evolution – objectives already central to heavy-ion physics. By systematically studying a selected set of isobaric or isobar-like nuclei with well-known structural properties, we can establish crucial “lever arms” to refine this method. Calibrating the technique with these benchmark systems ensures that the three steps of the imaging framework are validated and improved. This calibration is crucial for probing the many-body nuclear wavefunction at high energies, imposing stricter constraints on the QGP’s initial conditions, as well as its dynamics and properties.

Once calibrated, imaging-by-smashing can be a powerful tool for exploring the ground-state structure of atomic nuclei. By colliding species whose shape parameters are difficult to determine through low-energy methods and analyzing the resulting heavy-ion observables, nuclear shapes can be directly extracted. This technique operates on extremely short timescales, enabling the differentiation between nuclei with rigid, stable shapes and those that exhibit rapid fluctuations. Moreover, the large number of charged particles produced in each event facilitates the study of higher-order nuclear deformations, including octupole and hexadecapole shapes, through measurements of higher-order flow harmonics.

This method can also help address fundamental questions in nuclear physics. For instance, it may reduce theoretical uncertainties in neutrinoless double-beta de-

cay searches ($0\nu\beta\beta$) [18], a process highly sensitive to the similarity of nuclear shapes in parent-daughter isobaric pairs. By comparing collisions of these nuclei, the technique can precisely quantify shape differences, thereby improving decay rate predictions. Furthermore, it opens new avenues for studying alpha clustering in light isobar-like systems such as $^{16}\text{O}+^{16}\text{O}$ and $^{20}\text{Ne}+^{20}\text{Ne}$ [19], providing stringent tests for *ab initio* nuclear theories.

Various collider facilities offer further opportunities to develop this imaging method. For example, the NICA collider operates at lower center-of-mass energies ($\lesssim 10$ GeV). It can collide a wide range of species, offering insights into how nuclear structure evolves across different energies and timescales. At RHIC, existing datasets from collisions such as $^{96}\text{Ru}+^{96}\text{Ru}$ and $^{96}\text{Zr}+^{96}\text{Zr}$ remain valuable for refining the imaging approach.

Looking ahead, planned system scans at the LHC beyond Run 3 (post-2029) promise to broaden the scope of this technique. A new ion source could allow up to four different collision species per heavy-ion run, increasing the range of nuclei available for study. Additionally, the SMOG-2 system at the LHCb experiment [20] allows the LHC ion beam to collide with fixed targets, offering greater flexibility in selecting collision systems. These advancements underscore the imaging-by-smashing method’s potential to significantly advance our understanding of nuclear structure and heavy-ion physics across a broad range of energies.

The author would like to thank Aihong Tang for inviting him to present a BNL colloquium, which forms the basis of this note, as well as critical feedback from Giuliano Giacalone. This work is supported by the U.S. Department of Energy, Award number DE-SC0024602.

* Correspond to jiangyong.jia@stonybrook.edu

- [1] STAR Collaboration, *Nature* **635**, 67 (2024), [arXiv:2401.06625 \[nucl-ex\]](https://arxiv.org/abs/2401.06625).
- [2] X. F. Yang, S. J. Wang, S. G. Wilkins, and R. F. Garcia Ruiz, *Prog. Part. Nucl. Phys.* **129**, 104005 (2023).
- [3] W. Busza, K. Rajagopal, and W. van der Schee, *Ann. Rev. Nucl. Part. Sci.* **68**, 339 (2018).
- [4] S. Yun, *Scientific Reports* **7** (2017), 10.1038/s41598-017-18017-2.
- [5] K. M. O’Hara, S. L. Hemmer, M. E. Gehm, S. R. Granade, and J. E. Thomas, *Science* **298**, 2179 (2002), [arXiv:cond-mat/0212463](https://arxiv.org/abs/cond-mat/0212463).
- [6] Z. Vager, R. Naaman, and E. P. Kanter, *Science* **244**, 426 (1989).
- [7] R. Boll, J. M. Schäfer, B. Richard, K. Fehre, G. Kastirke, Z. Jurek, and et al., *Nature Physics* **18**, 423 (2022).
- [8] U. W. Heinz, *J. Phys. Conf. Ser.* **455**, 012044 (2013), [arXiv:1304.3634 \[nucl-th\]](https://arxiv.org/abs/1304.3634).
- [9] S. Bhatta, C. Zhang, and J. Jia, *Phys. Lett. B* **858**, 139034 (2024), [arXiv:2301.01294 \[nucl-th\]](https://arxiv.org/abs/2301.01294).
- [10] J. Jia, *Phys. Rev. C* **105**, 014905 (2022), [arXiv:2106.08768 \[nucl-th\]](https://arxiv.org/abs/2106.08768).
- [11] H. Niemi, G. S. Denicol, H. Holopainen, and P. Huovinen, *Phys. Rev. C* **87**, 054901 (2013).
- [12] P. Bożek and W. Broniowski, *Phys. Rev. C* **85**, 044910 (2012).
- [13] J. E. Bernhard, J. S. Moreland, and S. A. Bass, *Nature Phys.* **15**, 1113 (2019).
- [14] J. Jia *et al.*, *Nucl. Sci. Tech.* **35**, 220 (2024), [arXiv:2209.11042 \[nucl-ex\]](https://arxiv.org/abs/2209.11042).
- [15] G. Giacalone, *Phys. Rev. Lett.* **124**, 202301 (2020), [arXiv:1910.04673 \[nucl-th\]](https://arxiv.org/abs/1910.04673).
- [16] J. Jia, *Phys. Rev. C* **105**, 044905 (2022), [arXiv:2109.00604 \[nucl-th\]](https://arxiv.org/abs/2109.00604).
- [17] G. Nijs and W. van der Schee, (2023), [arXiv:2304.06191 \[nucl-th\]](https://arxiv.org/abs/2304.06191).
- [18] M. Agostini, G. Benato, J. A. Detwiler, J. Menéndez, and F. Vissani, *Rev. Mod. Phys.* **95**, 025002 (2023), [arXiv:2202.01787 \[hep-ex\]](https://arxiv.org/abs/2202.01787).
- [19] G. Giacalone *et al.*, (2024), [arXiv:2402.05995 \[nucl-th\]](https://arxiv.org/abs/2402.05995).
- [20] LHCb Collaboration, 10.17181/CERN.SAQC.EOWH.